Phylogeny of Amphidinium (Dinophyceae) from Guam and Okinawa, with descriptions of A. pagoense sp. nov . and A. uduigamense sp. nov.

Article *in* Phycologia · April 2022

DOI: 10.1080/00318884.2022.2033948

CITATIONS
0

READS
52

4 authors, including:

Filip Husnik
Okinawa Institute of Science and Technology
71 PUBLICATIONS **1,423** CITATIONS

SEE PROFILE

Sarah Lemer
University of Guam
147 PUBLICATIONS **847** CITATIONS

SEE PROFILE

Kevin Wakeman
Hokkaido University
68 PUBLICATIONS **308** CITATIONS

SEE PROFILE

Phycologia

Phycologia

ISSN: (Print) (Online) Journal homepage: https://www.tandfonline.com/loi/uphy20

Phylogeny of *Amphidinium* (Dinophyceae) from Guam and Okinawa, with descriptions of *A. pagoense sp. nov*. and *A. uduigamense sp. nov.*

Yong Heng Phua, Filip Husnik, Sarah Lemer & Kevin C. Wakeman

To cite this article: Yong Heng Phua, Filip Husnik, Sarah Lemer & Kevin C. Wakeman (2022): Phylogeny of *Amphidinium* (Dinophyceae) from Guam and Okinawa, with descriptions of *A. pagoense sp. nov*. and *A. uduigamense sp. nov.*, Phycologia, DOI: 10.1080/00318884.2022.2033948

To link to this article: https://doi.org/10.1080/00318884.2022.2033948

PHYCOLOGIA
https://doi.org/10.1080/00318884.2022.2033948

Phylogeny of *Amphidinium* (Dinophyceae) from Guam and Okinawa, with descriptions of *A. pagoense sp. nov.* and *A. uduigamense sp. nov.*

Yong Heng Phua[1,2], Filip Husnik[2], Sarah Lemer[3] and Kevin C. Wakeman[4]

[1]*School of Science, Hokkaido University, North 10, West 8, Sapporo, 060-0810, Japan*
[2]*Okinawa Institute of Science and Technology Graduate University, 1919-1 Tancha, Onna-son, 904-0495, Japan*
[3]*University of Guam Marine Laboratory, 303 University Drive, UOG Station, Mangilao, GU 96923, USA*
[4]*Institute for the Advancement of High Education, Hokkaido University, North 10, West 8, Sapporo, 060-0810, Japan*

ABSTRACT

Marine benthic dinoflagellates within the genus *Amphidinium* were isolated from Guam and Okinawa. Isolated strains were identified to species-level using phylogenetic analyses of 28S rRNA and ITS-5.8S rRNA genes as well as microscopy. Of the six isolated strains, two were new species: *A. pagoense sp. nov.* and *A. uduigamense sp. nov.* Other isolates included strains of *A. massartii* and *A. operculatum* from Guam, and two strains of *A. operculatum* from Okinawa. Both new species were described using light and electron microscopy (SEM and TEM). The combination of characteristics that make *A. pagoense sp. nov.* unique includes a pair of centrally-located pyrenoids, variable cell shape, absence of scales and a long, curved ventral ridge. For *A. uduigamense sp. nov.*, a combination of several morphological features distinguishes it from other species. These include a constriction near the anterior of the hypocone, two centrally located pyrenoids, a longitudinal flagellum inserted in the posterior one-third of the cell, cell size, cell division in the motile stage and the absence of scales. Toxicity was confirmed in these two novel species by testing methanol extracts in an *Artemia* bioassay. Previously unrecorded ITS rRNA gene sequences from *A. operculatum* were also sequenced from both locations. Species identified and newly described in this study expand the taxonomic knowledge of *Amphidinium* in the Pacific.

ARTICLE HISTORY
Received 17 September 2021
Accepted 22 January 2022
Published online 19 April 2022

KEYWORDS
Biodiversity; Epiphytic dinoflagellates; Microalgae; Molecular phylogeny; Taxonomy

INTRODUCTION

The genus *Amphidinium* Claparède & J. Lachmann is a group of globally distributed athecate dinoflagellates (Nakajima *et al.* 1981; Dodge 1982; Flø Jørgensen *et al.* 2004; Dolapsakis & Economou-Amilli 2009). They are often found in tropical and subtropical waters living epiphytically on macroalgae or benthically within sediment (Daugbjerg *et al.* 2000; Murray & Patterson 2002; Rhodes *et al.* 2014). *Amphidinium sensu stricto* was redefined using both morphological and molecular markers (Steidinger & Tangen 1997; Flø Jørgensen *et al.* 2004). Morphological features such as a left-deflecting, small epicone less than one-third of the cell length, as well as molecular phylogenetics mainly based on 28S rRNA gene (hereafter 28S) datasets, have been used to adjust the systematics of the group, establishing the Amphidiniaceae in the order Amphidiniales (Flø Jørgensen *et al.* 2004; Moestrup & Calado 2018).

The type species, *A. operculatum*, was first described by Claparède & Lachmann (1859). This original description was based on cell shape, sulcus position and an orange-red pigmented body referred to as 'stigma' (Grell & Wohlfarth-Bottermann 1957; Murray & Patterson 2002; Flø Jørgensen *et al.* 2004). The lack of adequate descriptions as well as the morphological variability within the group caused species within this genus to be arbitrarily classified (Taylor 1971; Murray *et al.* 2004). This taxonomic confusion has hindered a proper understanding of the group's diversity. In addition, many overlapping characteristics such as metabolic movement and scale production have made it difficult to identify individual species based solely on a single morphological feature (Flø Jørgensen *et al.* 2004; Murray *et al.* 2004; Dolapsakis & Economou-Amilli 2009). Karafas *et al.* (2017) used a combination of morphology and molecular analyses (phylogenetic, secondary structure and compensatory base changes) to delineate species in the 'operculatum' clade.

Amphidinium is of particular interest as some species have been shown to produce bioactive compounds like amphidinols (Morsy *et al.* 2008; Espiritu *et al.* 2017; Martínez *et al.* 2019), amphidinolides (Kobayashi & Tsuda 2004) and luteophanol A-like compounds (Murray *et al.* 2015) in both lab-grown cultures and natural blooms. Some of these compounds are toxic to human cancer cell lines, marine vertebrates and invertebrates (Bates *et al.* 1978; Yasumoto *et al.* 1987; Baig *et al.* 2006; Murray *et al.* 2012, 2015; Karafas *et al.* 2017). Others showed antifungal and cytotoxic properties (Satake *et al.* 1991; Morsy *et al.* 2008; Espiritu *et al.* 2017; Martínez *et al.* 2019).

The widespread distribution and potential to produce harmful or useful compounds make it important to understand the biodiversity and taxonomy of *Amphidinium*. In the present study, strains of *Amphidinium* were isolated from understudied subtropical regions in the Pacific: Guam and

CONTACT Kevin C. Wakeman wakeman.k@oia.hokudai.ac.jp
Supplemental data for this article can be accessed on the publisher's website.

Okinawa. From six isolates, clonal cultures were established and identified using 28S and ITS rRNA gene markers as well as light microscopy, SEM and TEM. Their toxicity was confirmed using an *Artemia* bioassay.

MATERIAL AND METHODS

Sample collection and maintenance

Crude samples were collected from macroalgae and turf algae on coral reefs in Guam and three sampling sites in Okinawa, Japan (Table 1). Samples were bottled and separated into containers with half-concentration Daigo's IMK Medium (Wako Pure Chemical Industries, Japan) and incubated for two weeks at 25°C. Single cells were isolated using a glass capillary and transferred to 48-well plates containing half-concentration Daigo's IMK. Once the cultures were stable, and growth was visible with the naked eye, cultures were transferred and maintained in Petri dishes containing Daigo's IMK medium.

DNA extraction, PCR amplification and sequencing

Genomic DNA was extracted from five-cell isolates with 10 µl QuickExtract™ FFPE DNA Extraction Kit (Lucigen, Middleton, Wisconsin, USA) and incubated according to the manufacturer's protocol. The 28S D1–D3 region and ITS1-5.8S-ITS2 (hereafter ITS) genes were amplified and sequenced. Initial amplification was performed by amplifying the ribosomal operon (18S rRNA – 28S rRNA genes) using primers PF1–28-1483R (Daugbjerg *et al.* 2000; Leander *et al.* 2003) with Hotstart 2x Master Mix (Qiagen, Hilden, Germany). The initial reaction was diluted 100× and a second round of PCR was performed using nested primers and EconoTaq 2X Master Mix (Lucigen). The 28S D1+D2 and D3 regions were amplified using D1RF1–852R-70 and D3A–28-1483R primers with the following program on a thermocycler: initial denaturation 94°C for 2 min; 25 cycles of 94°C for 15s, 52°C for 15s, 72°C for 1 min 40s; final extension 72°C for 7 min. The ITS region was amplified with Lp1F1–25F1R or ITS specific primers (Amphioperc_ITSR: strains G3, I78, I85, and specific primer for *A. uduigamense sp. nov.*, I76_ITSR); the same thermocycler parameters used to amplify the 28S were used on the ITS region. Primer sequences are listed in Table S1.

After checking the size of the PCR products on a 1% agarose gel, they were purified with Polyethylene Glycol (PEG), then cycle-sequenced with BrilliantDye™ Terminator v1.1 (Nimagen, Nijmegen, Netherlands) according to the manufacturer's protocol, and sequenced on a 3130 genetic analyser (Applied Biosystems, Waltham, Massachusetts, USA). The National Center for Biotechnology Information's (NCBI) Basic Local Alignment Search Tool (BLAST) was used to check the sequences. Sequences obtained from this study were deposited in NCBI with the following accession numbers: MZ851798–MZ851806.

Table 1. Locations where crude samples of macroalgae and turf algae were collected.

Amphidinium sp.	Strain	Sampling site	Sampling date	Site coordinates
A. operculatum	G3	Guam	Mar. 2020	13°25.660′N, 144° 47.902′E
A. pagoense sp. nov.	G5	Guam	Mar. 2020	13°25.660′N, 144° 47.902′E
A. massartii	G12	Guam	Mar. 2020	13°25.660′N, 144° 47.902′E
A. uduigamense sp. nov.	I76	Okinawa	Feb. 2021	26°29.9317′N, 127° 50.53′E
A. operculatum	I78	Okinawa	Feb. 2021	26°30.145′N, 127° 54.633′E
A. operculatum	I85	Okinawa	Feb. 2021	26°26.145′N, 127° 54.5567′E

Phylogeny

Both ITS and 28S sequences were aligned using Muscle 3.8.31 (Edgar 2004) algorithm in Mesquite (Maddison & Maddison 2021) with other *Amphidinium* and *Gyrodinium* sp. (the latter used as outgroup) sequences retrieved from GenBank (Tables S2, S3). Alignments were trimmed using Gblocks v0.91b (Castresana 2000; Talavera & Castresana 2007). The final alignments for 28S and ITS consisted of 115 sequences, containing 671 aligned nucleotides and 91 sequences with 654 aligned nucleotides, respectively.

IQ-TREE v1.6.12 (Nguyen *et al.* 2014) was used to select the GTR+Γ+G4 substitution model following Akaike Information Criterion with correction. Maximum-likelihood (ML) bootstrap analysis was then performed on 1000 pseudoreplicates.

Bayesian analysis was performed with MrBayes v3.2.7 (Ronquist & Huelsenbeck 2003). Four Markov chain Monte Carlo (MCMC) chains were run for 50,000,000 generations and sampled every 100th generation. Parameters were set to the General Time Reversible (GTR) substitution model with the rate variation across sites set to a proportion of invariable sites modelled by a gamma distribution (lset rates = invgamma). Other parameters were set to default settings. Tracer 1.7 (Rambaut *et al.* 2018) was used to check chain convergence.

MEGA-X (Kumar *et al.* 2018) was used to calculate the pairwise distances between 28S sequences. Program parameters were set to 1000 bootstrap; *p*-distance with transition and transversions; evolutionary rates among sites were set as gamma-distributed.

Microscopy

For light and epifluorescence microscopy, live cells and cells fixed in 2.5% glutaraldehyde with DAPI (0.1 µg ml^{-1}), were mounted on glass slides. The slides were viewed under a Zeiss Axioskop 2 plus (Zeiss, Oberkochen, Germany) microscope and imaged with a Canon EOS Kiss X8i camera (Canon, Tokyo, Japan). Two fixation techniques were used for SEM. *Amphidinium pagoense sp. nov.* was fixed in 2.5% glutaraldehyde for 30 min and then 2% OsO_4 for 30 min; other samples were fixed with 2% OsO_4 for 20 min. Cells were rinsed with filtered seawater and distilled water three times each, then dehydrated with a stepwise increase in the concentration of ethanol (70%, 80%, 90%, 95% and

3 × 100%) for 5 min at each step. *Amphidinium pagoense sp. nov.* was then freeze-dried with t-butyl alcohol and mounted on stubs, sputter-coated for 4 min with gold, then viewed using a JSM-7900F (Jeol, Tokyo, Japan) microscope. Other samples were critical point dried using a Leica EM CPD300 (Leica, Wetzlar, Germany), mounted on stubs, sputter-coated for 4 min with gold, then viewed using a Hitachi *N*-3000 (Hitachi, Tokyo, Japan) microscope.

For TEM, a dense culture of cells was spun down into a pellet in a 1.5-ml Eppendorf tube then fixed with a mixture of 2% glutaraldehyde and 1% OsO_4 in seawater for 15 min. Cells were rinsed with filtered seawater and postfixed with 1% OsO_4 for 1 h, then rinsed with filtered seawater and distilled water three times for 5 min each. The cells were dehydrated with a stepwise increase in the concentration of ethanol (70%, 80%, 90%, 95% and 100%) for 5 min at each step. Permeabilization was performed with a 1:1 acetone:ethanol mixture for 2 min then 100% acetone twice for 5 min, and allowed to sit in 2:1 acetone:resin mixture for 2 h. The mixture was exchanged with resin twice, and polymerized at 70°C for 30 h. Samples were cut into 50-nm sections with a diamond knife and imaged using a Hitachi-7400 transmission electron microscope.

Methanol extraction

Methanol extractions were performed from 1 l of dense culture material that was vacuum-filtered through Whatman® 1825-042 GF/F Glass Microfiber Filters (Merck, Darmstadt, Germany) and subsequently stored at −80°C. Cells were allowed to thaw before the addition of 5 ml of methanol. The filters were spun down and sonicated for 5 min. Cells were then left at room temperature with occasional shaking for 30 min. Extractions were repeated a total of four times and the final extraction was left overnight. Evaporation of methanol solvent from the extractions was done using a rotary evaporator (AS ONE, Osaka, Japan) and stored at −20°C. Desalting was performed using Supel™-Select HLB 1 ml tubes (Merck). Tubes were first activated using 1 ml MeOH, then samples were dissolved using aqueous-methanol (9 water:1 methanol) and passed over the HLB column. Retained samples were washed with 1 ml aqueous-methanol (9 water:1 methanol) twice, then eluted with 1 ml MeOH, dried in a rotary evaporator and stored at −20°C.

Artemia bioassay

Artemia eggs were allowed to hatch in 0.22-µm–filtered seawater. After 24 h, *Artemia* nauplii were transferred into wells with 475 µl of filtered seawater. Desalted extracts (1 mg) were dissolved in 100 µl DMSO 1% (v/v) and 25 µl were added to each well to a total volume of 500 µl. Three replicates were made (total n = 30). Wells were observed and *Artemia* recorded at 12, 24, 48 and 72 h intervals.

RESULTS

Species descriptions

Amphidinium pagoense Phua & Wakeman *sp. nov.*
Figs 1–17

DIAGNOSIS: Athecate, oval to round autotrophic dinoflagellate. Minute left-deflecting, crescent-shaped epicone. Two pyrenoids centrally located side by side. Pusules centrally located in the hypocone. Nucleus in the posterior part of the hypocone. Antapex variable, round to slightly pointed.

DESCRIPTION: Cells oval to round with an average length of 23.93 ± 2.96 µm (range 17.0–32.4 µm, n = 30) and width of 18.76 ± 3.69 µm (range 13.4–29.4 µm, n = 30) (Figs 1–12). Epicone crescent-shaped, pointing to the left (Fig. 4). Cell shape variable, oval cells with slightly pointed antapex, round cells with rounded antapex (Figs 1, 2, 4–7). Anterior hypocone symmetry variable depending on cell shape, symmetrical in round cells, in oval cells right margin convex and left margin slightly concave (Figs 1, 2, 5–7). Cell division observed in the motile stage (Fig. 8). Chloroplast lobes densely grouped around epicone and anterior portion of hypocone, sparse around the nucleus (Figs 3, 9). Nucleus bean-shaped, located posteriorly in hypocone (Fig. 10). Transverse flagellum inserted in the cingulum, at the right side of the epicone (Fig. 4). Ventral ridge long, curved, connecting the sulcus to the cingulum (Fig. 12). Longitudinal flagellum inserted in the middle of the sulcus (Fig. 12). Cell surface covered in roughly hexagonal amphiesmal vesicles (Fig. 13). Scales not observed on the cell surface (Figs 14, 15). Two pusules, one located in the middle-anterior part of the hypocone and another in the middle of the cell (Figs 1, 6, 16). Two pyrenoids located centrally in the cell often surrounded by starch (Figs 1, 2, 5, 14, 17). Metabolic movement was not observed. Cyst formation during division not observed in culture. Toxicity detected with *Artemia* bioassay. ITS rRNA gene GenBank accession: MZ851802; 28S rRNA gene GenBank accession: MZ851803.

HOLOTYPE: Fixed and dried specimens on SEM stub (storage name: G5), held in the Biodiversity Lab associated with the Hokkaido University Museum.

REFERENCE MATERIAL: Living cultures deposited in NIES microbial culture collection (culture name: G5).

TYPE LOCALITY: Pago Bay, Guam, 13°25.660′N, 144°47.902′E.

HABITAT: Marine, epiphytic and benthic habitats.

ETYMOLOGY: The specific epithet refers to the type locality, Pago Bay, Guam, from where it was isolated.

Amphidinium uduigamense Phua & Wakeman *sp. nov.*
Figs 18–32

DIAGNOSIS: Athecate, autotrophic dinoflagellate. Cell oval, with minute left-deflecting flat epicone. Constriction at the anterior fifth of hypocone, forming an indentation. Two pyrenoids centrally located side by side. Pusules centrally located in the hypocone. Nucleus in the posterior part of the hypocone. Antapex somewhat rounded.

DESCRIPTION: Cells ovoid, with average length of 39.12 ± 2.57 µm (range 34.9–44.1 µm, n = 22) and width of 30.37 ± 3.46 µm (range 26.5–37.9 µm, n = 22) (Figs 18–26). Flat epicone slightly deflecting to the left (Fig. 20). Anterior end of hypocone symmetrical, usually overlapping the posterior margin of the cingulum, raised into a collar shape. A shallow dent, located *c.* $^1/_5$ of the hypocone's length from its anterior end, forms a V-shape in ventral view (Figs 18, 20, 21, 25). Cells widest at the middle and with

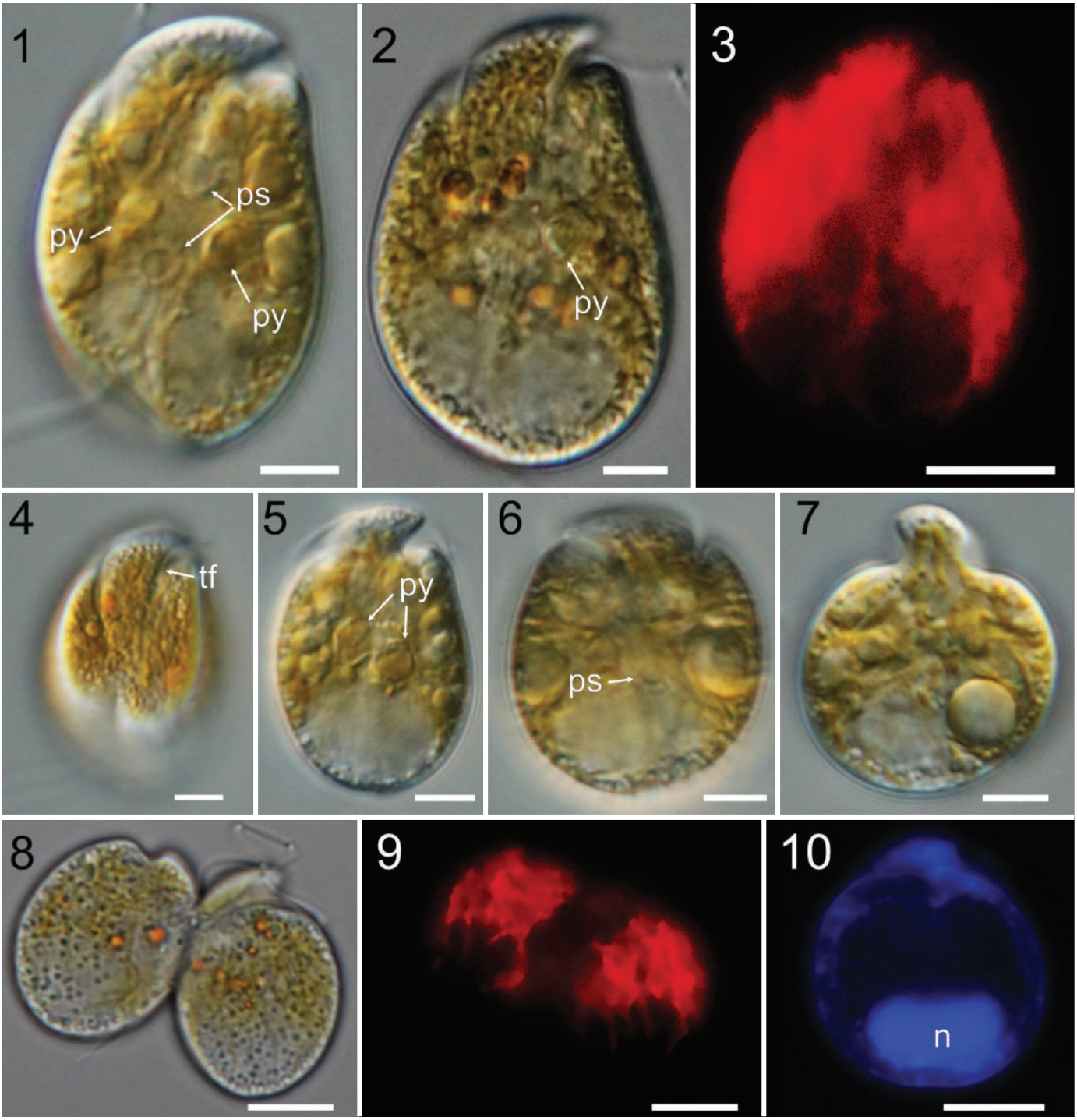

Figs 1–10. *Amphidinium pagoense sp. nov.*, bright field and fluorescence LM.
Fig. 1. Ovoid cell with pyrenoids (py) and pusules (ps). Scale bar = 5 µm.
Fig. 2. Ovoid cell with pyrenoid (py). Scale bar = 5 µm.
Fig. 3. Ovoid cell displaying plastid epifluorescence. Scale bar = 10 µm.
Fig. 4. Cell surface, showing epicone and transverse flagellum (tf). Scale bar = 5 µm.
Fig. 5. Ovoid cell with asymmetric anterior hypocone, round antapex and pyrenoids (py). Scale bar = 5 µm.
Fig. 6. Round cell with pusule (ps). Scale bar = 5 µm.
Fig. 7. Round cell (note: the culture contained cells of variable cell shape). Scale bar = 5 µm.
Fig. 8. Late division stage. Scale bar = 10 µm.
Fig. 9. Epifluorescence of plastids in dividing cells. Scale bar = 10 µm.
Fig. 10. DAPI-stained round cell, showing nucleus (n). Scale bar = 10 µm.

a somewhat rounded antapex (Figs 18, 20, 21, 24–26). Chloroplasts radiating throughout the cell with periodic thicker nodes visible in the hypocone (Figs 18–22). Nucleus oval, near the cell antapex (Fig. 23). Transverse flagellum in the cingulum, originating next to the ventral ridge (Fig. 20). Sulcus visible at the posterior one-third of the hypocone, from where longitudinal flagellum emerges (Figs 24, 25, 27). Ventral ridge short and

Figs 11–13. *Amphidinium pagoense sp. nov.*, SEM.
Fig. 11. Whole cell with flagella and hexagonal surface structures. Scale bar = 5 µm.
Fig. 12. Group of cells, with the transverse and longitudinal flagella (white arrows) and the ventral ridge (*) indicated. Scale bar = 10 µm.
Fig. 13. High magnification showing the limits of the roughly hexagonal amphiesmal vesicles on the cell surface Scale bar = 1 µm.

straight (Figs 20, 25). Pusules observed near centre of hypocone (Fig. 18). Scales not observed on the cell surface (Figs 28, 29). Chloroplasts radiating from two centrally located pyrenoids, which are occasionally surrounded by starch (Figs 18, 19, 21, 22, 31, 32). Metabolic movement not observed. Cell division in the motile stage. Division cyst formation not observed in culture. Toxicity detected with *Artemia* bioassay. ITS rRNA gene GenBank accession: MZ851800; 28S rRNA gene GenBank accession: MZ851801.

HOLOTYPE: Fixed and dried specimens on SEM stub (storage name: I76), held in the Biodiversity Lab associated with the Hokkaido University Museum.

REFERENCE MATERIAL: Living cultures deposited in NIES microbial culture collection (culture name: I76).

TYPE LOCALITY: Uduigama, Okinawa, 26°30.145′N, 127°50.633′E.

HABITAT: Marine, epiphytic and benthic habitats.

ETYMOLOGY: The specific epithet refers to the type locality, Uduigama, Okinawa, Japan, from where it was isolated.

Amphidinium operculatum strains G3, I78 and I85
Figs 33–38

DESCRIPTION: *Amphidinium operculatum* strains G3, I78 and I85 showed a similar morphology (Figs 33–38). Ovoid cells with small, left-deflected triangular epicone. Anterior end of hypocone asymmetrical, with left side more concave than right. Longitudinal flagellum emerging into visible part of the sulcus near the posterior end of the cell. Nucleus oval, at the posterior part of the hypocone. Orange-red pigmented body above nucleus observed, reminiscent of a 'stigma' (Figs 33, 35, 37).

Amphidinium massartii strain G12
Figs 39, 40

DESCRIPTION: Cell shape ellipsoidal, with crescent-shaped, minute epicone (Figs 39, 40). One central pyrenoid commonly found (Fig. 39), rarely two pyrenoids: one central, one lateral. Oval nucleus located posteriorly. Occasionally, small reddish bodies are located in hypocone. Large amounts of mucilage produced in culture.

Molecular phylogeny

Sequences obtained from 28S and ITS gene regions were aligned and analysed. *Amphidinium pagoense* from Guam was sister to *A. magnum* Karafas & Tomas with high bootstrap support (bs) and Bayesian posterior probability (pp) for both 28S (100/1) and ITS (99/1) trees (Figs 41, 42). In the 28S phylogeny, strains G3, I78 and I85 grouped with *A. operculatum* with maximum support (Fig. 41). No previous ITS sequences from *A. operculatum* were recorded in GenBank but strains G3, I78 and I85 formed a strongly supported group (Fig. 42). In the 28S phylogeny, *A. uduigamense* was sister to *Amphidinium* sp. strain AmGMM3 with maximum support for both bs and pp. In the ITS phylogeny, sequence records for *Amphidinium* sp. strain AmGMM3 and *A. incoloratum* P.H. Campbell are not available; in this tree, *A. uduigamense* was sister to the *A. operculatum* clade (strains G3, I78 and I85) with low support. Both 28S and ITS phylogenies showed *A. uduigamense, Amphidinium* sp. strain AmGMM3 and *A. operculatum* to have long branches (distance >0.4) compared to the other species in the genus. Strain G12 grouped with strong

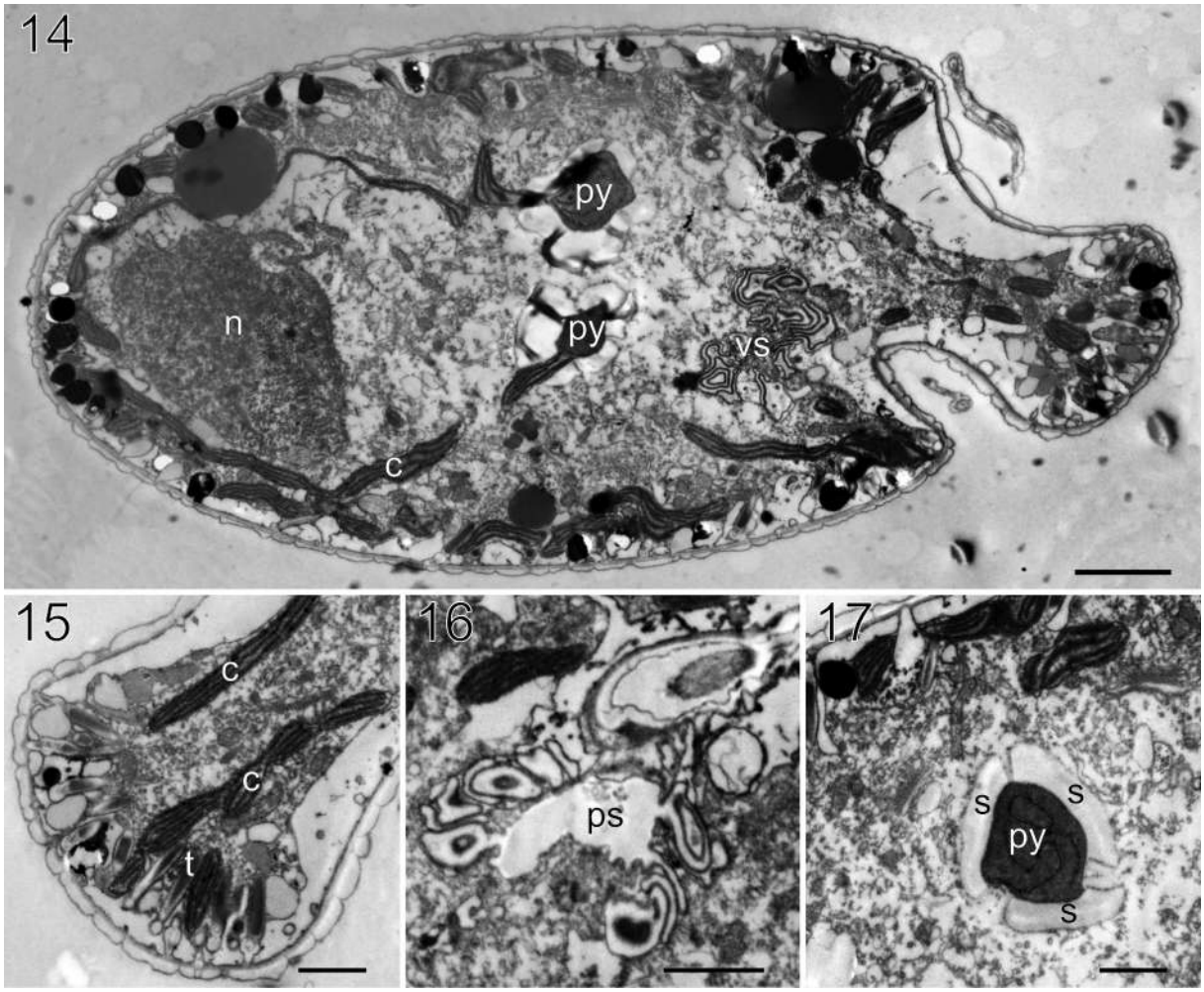

Figs 14–17. *Amphidinium pagoense sp. nov.*, TEM, longitudinal sections. Nucleus (n); chloroplast (c); pyrenoids (py); trichocyst (t); vesicular structures (vs); pusules (ps); starch granules (s).

Fig. 14. Longitudinal section of the cell showing general shape. Scale bar = 2 µm.

Fig. 15. Section of the epicone with amphiesmal vesicles on the cell surface. Scale bar = 1 µm.

Fig. 16. High magnification of the centrally-located pusule. Scale bar = 1 µm.

Fig. 17. High magnification of the pyrenoid surrounded by starch granules. Scale bar = 1 µm.

support together with other strains of *A. massartii* Biecheler in 28S and ITS phylogenies.

Intraspecific variation, as estimated from *p*-distances calculated for available 28S sequences, ranged from 0.0 to 0.038, with the highest distance found for *A. operculatum* (Table 2). Interspecific *p*-distances varied between 0.040 and 0.425; the *p*-distances between *A. pagoense* and *A. magnum*, and between *A. uduigamense* and *Amphidinium* sp. strain AmGMM3, were 0.08 and 0.316, respectively (Table 2). Similar to *A. operculatum, A. uduigamense* had a high genetic distance from other species of the genus (>0.29).

Toxicity

Artemia bioassays were performed on nauplii and viability was decided based on motility. During the first 12 h after adding extracts, there seemed to be no effect on *Artemia*. However, after 24 h, 13% and 23% mortality were detected in wells with *A. pagoense* and *A. uduigamense* extracts, respectively (Fig. 43). At 48 h, >50% of *Artemia* nauplius were dead, whereas wells with DMSO (control) had only one death (7%). After 72 h, only 7% of *Artemia* were alive in wells that had extracts added (Fig. 43; Video S1).

DISCUSSION

The genus *Amphidinium* is distinguished from other athecate dinoflagellates by its small (<⅓ cell size), left-deflected epicone and the posteriorly located nucleus (Flø Jørgensen *et al.* 2004). Within the genus, varying morphological differences and overlapping characteristics of the species had made teasing apart individual species of *Amphidinium* difficult (Flø Jørgensen *et al.* 2004; Murray *et al.* 2004; Table S4). The type species, *A. operculatum*, is unique among the photosynthetic species because it lacks a starch-sheathed pyrenoid and it has a posteriorly located sulcus (Murray *et al.* 2004); other plastid-bearing *Amphidinium* species contain at least one pyrenoid (Flø Jørgensen *et al.* 2004; Murray *et al.* 2004, 2012; Dolapsakis & Economou-Amilli 2009). Typically, a combination of morphological characteristics was used for the classification of species. The

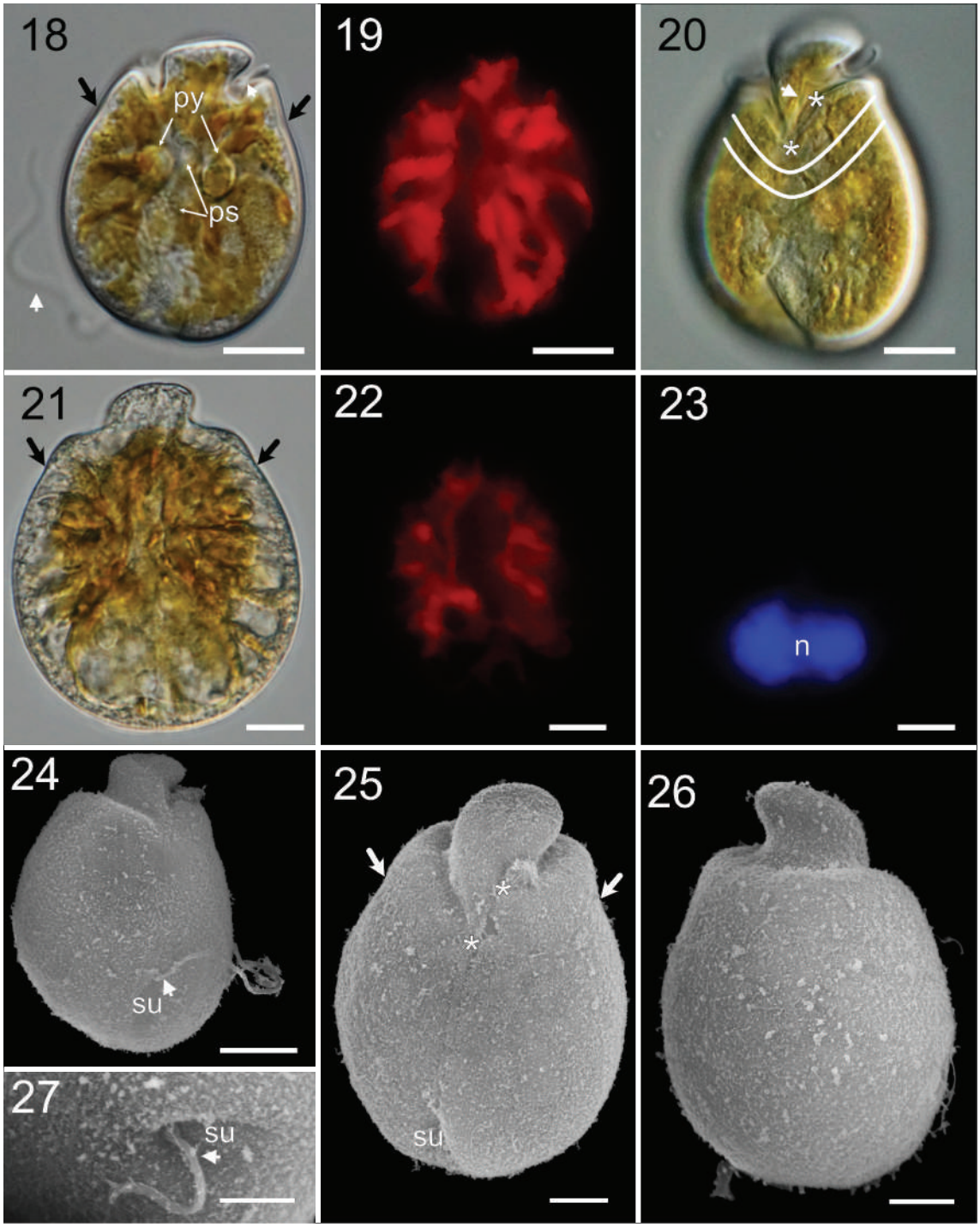

Figs 18–27. *Amphidinium uduigamense sp. nov.*, bright field and fluorescence LM, and SEM.

Fig. 18. Ovoid cell in LM, with two pyrenoids (py) near the middle of the cell, pusules (ps), flagella (white arrows) and lateral indentation (black arrows). Scale bar = 10 µm.

Fig. 19. Epifluorescence of the chloroplasts radiating from the pyrenoid. Scale bar = 10 µm.

Fig. 20. Cell surface showing the ventral ridge (*) and V-shaped indentation (with limits indicated by the white lines). The white arrow points to the base of the transverse flagellum. Scale bar = 10 µm.

Fig. 21. Dorsal view of the cell. Black arrows show indentation. Scale bar = 10 µm.

Fig. 22. Epifluorescence of the dorsal view of plastid. Scale bar = 10 µm.

Fig. 23. DAPI-stained nucleus (n). Scale bar = 10 µm.

Fig. 24. SEM of cell in ventral view, showing the sulcus (su) and emergence of longitudinal flagellum (white arrow). Scale bar = 10 µm.

Fig. 25. SEM of cell in ventral view, showing the sulcus (su), ventral ridge (*), and indentation (white arrow). Scale bar = 5 µm.

Fig. 26. SEM of cell in dorsal view. Scale bar = 5 µm.

Fig. 27. High magnification SEM of the cell surface, showing emergence point of the longitudinal flagellum (white arrow). su, sulcus. Scale bar = 5 µm.

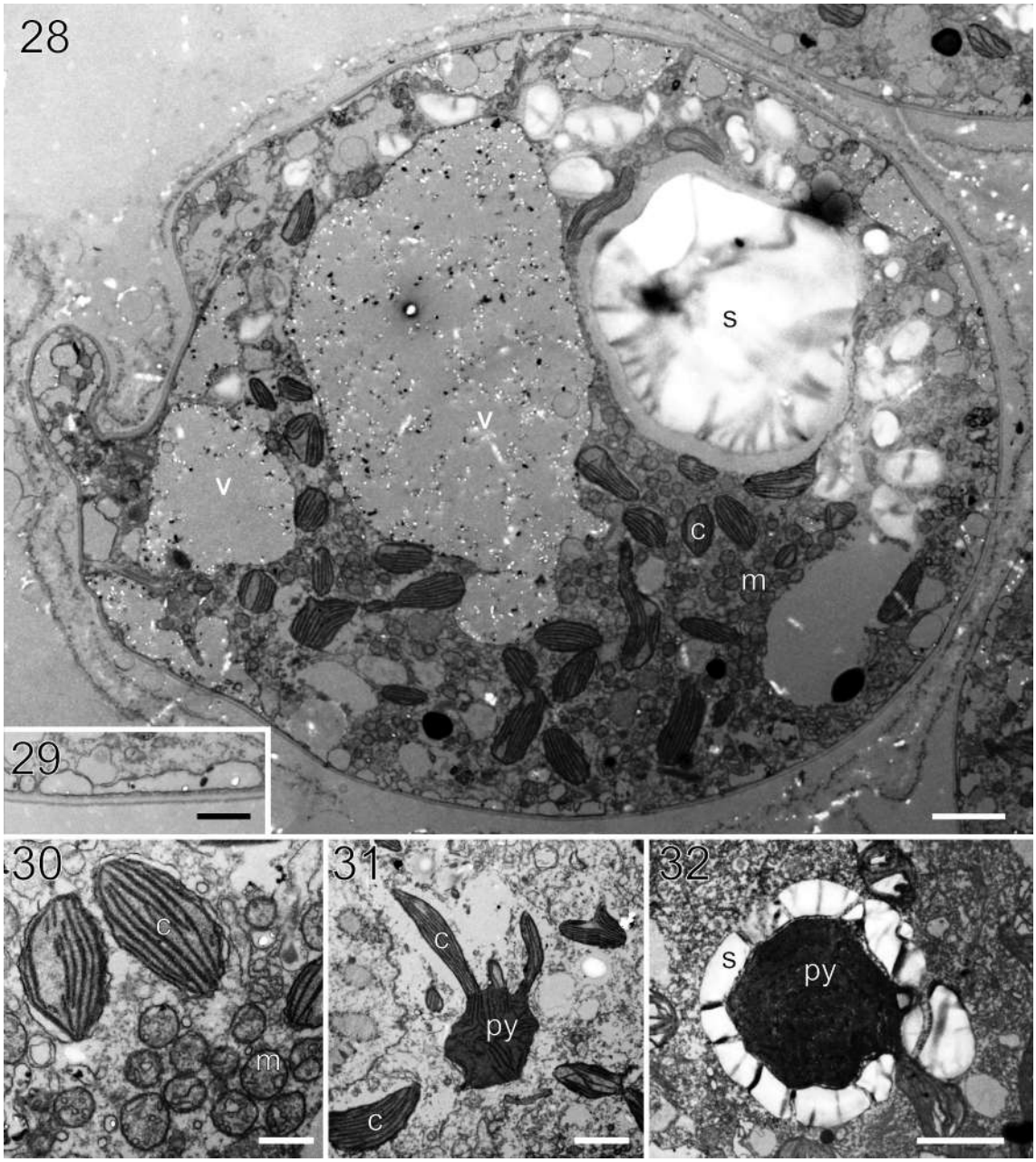

Figs 28–32. *Amphidinium uduigamense sp. nov.*, TEM, longitudinal sections, showing starch granules (s), vesicles (v), chloroplast lobes (c), pyrenoids (py) and mitochondria (m).

Fig. 28. Longitudinal section of cell showing the general shape and structure. Scale bar = 2 µm.

Fig. 29. High magnification of the cell surface. Scale bar = 500 nm.

Fig. 30. High magnification showing clusters of chloroplasts and mitochondria. Scale bar = 500 nm.

Fig. 31. Chloroplast lobes radiating from the pyrenoid. Scale bar = 2 µm.

Fig. 32. Pyrenoid surrounded by starch granules. Scale bar = 2 µm.

presence of scales on the cell surface, metabolic movement, length and shape of the ventral ridge, pyrenoid location, formation of dividing cysts, and the location of the insertion of the longitudinal flagella in the hypocone are important characteristics currently used for species identification (Murray *et al.* 2004, 2012; Lee *et al.* 2013; Karafas *et al.* 2017). Despite the variability within each species, the relative stability of characteristics such as size, cell shape, shape of the antapex and of the epicone and the symmetry of the anterior end of the hypocone are often used together to aid in the definition of species boundaries.

Amphidinium pagoense is generally smaller (17–32 µm) than *A. magnum* (26–47 µm). Moreover, the pyrenoids of *A. pagoense* are aligned side by side in the middle of the cell; those of *A. magnum* are lateral and vertically aligned (Karafas *et al.* 2017). The description of *A. magnum* did not include TEM, which would be needed to confirm the presence

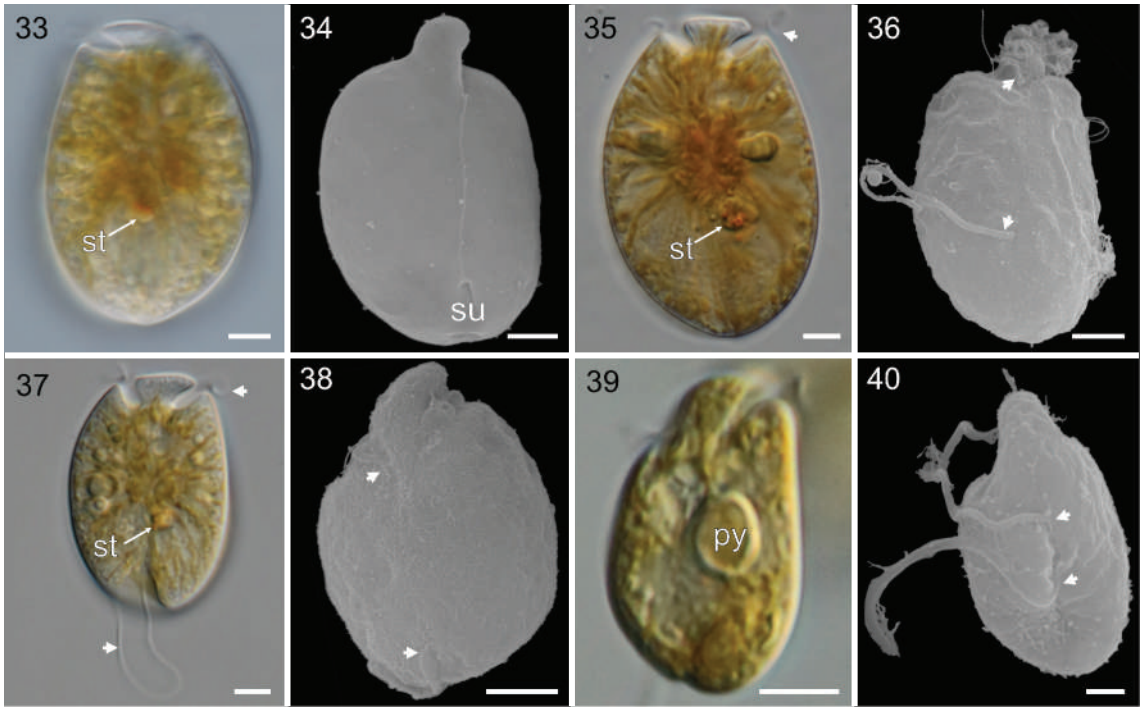

Figs 33–40. *Amphidinium operculatum* and *A. massartii*, LM and SEM, showing flagella (white arrows), pyrenoids (py) and 'stigma' (st).
Fig. 33. Light micrograph of the dorsal side of *A. operculatum* strain G3. Scale bar = 2 µm.
Fig. 34. SEM of the ventral view of *A. operculatum* strain G3, showing sulcus (su) at posterior end of cell. Scale bar = 5 µm.
Fig. 35. Light micrograph of the ventral side of *A. operculatum* strain I78. Scale bar = 5 µm.
Fig. 36. SEM of the ventral side of *A. operculatum* strain I78, showing longitudinal and transverse flagella (white arrows). Scale bar = 5 µm.
Fig. 37. Light micrograph of the ventral side of *A. operculatum* strain I85. Scale bar = 5 µm.
Fig. 38. SEM of ventral side of *A. operculatum* strain I85, showing longitudinal and transverse flagella (white arrows). Scale bar = 5 µm.
Fig. 39. Light micrograph of the ventral side of *A. massartii* strain G12. Scale bar = 5 µm.
Fig. 40. SEM of ventral side of *A. massartii* strain G12 showing longitudinal and transverse flagella (white arrows). Scale bar = 2 µm.

on the cell surface (Karafas *et al.* 2017). However, the absence of scales in *A. pagoense* separates it from *A. massartii, A.* cf. *massartii, A. theodorei* Tomas & Karafas ('*theodori*') and *A. paucianulatum* Karafas & Tomas (Murray *et al.* 2004; Lee *et al.* 2013; Karafas *et al.* 2017). Division in the motile stage and lack of metabolic movement distinguish *A. pagoense* from *A. steinii* (Lemmermann) Kofoid & Swezy, *A. thermaeum* Dolapsakis & Economou-Amilli, *A. theodorei* and *A. fijiense* Karafas & Tomas ('*fijiensis*') (Flø Jørgensen *et al.* 2004; Dolapsakis & Economou-Amilli 2009; Karafas *et al.* 2017). The long-curved ventral ridge makes it distinguishable from *A. carterae* Hulburt, *A. trulla* Sh. Murray, Lesley Rhodes & M. F. Jørgensen, *A. theodorei, A. fijiense, A. paucianulatum* and *A. pseudomassartii* Karafas & Tomas (Biecheler 1952; Flø Jørgensen *et al.* 2004; Murray *et al.* 2004; Dolapsakis & Economou-Amilli 2009; Lee *et al.* 2013; Karafas *et al.* 2017). The phylogenetic analyses reported herein placed *A. pagoense* as sister species to *A. magnum*, and within the clade formed by *A. magnum, A.* cf. *thermaeum, A. thermaeum* and *A. theodorei*. This expands our understanding of the clade adding on to previous studies of these species using 28S and ITS sequences (Karafas *et al.* 2017). Still, unique morphological features exclusively found in this group are not observable without direct comparison between cultures using identical sample preparation methods.

In *A. uduigamense*, a shallow dent forming a V-shaped constriction was consistently observed on the anterior fifth of the hypocone. This feature was not observed in other described species of *Amphidinium*. Other characteristics, like the presence of two pyrenoids in *A. uduigamense*, also distinguish it from *A. operculatum, A. massartii* and *A. gibbosum* (Murray *et al.* 2004). The emergence of the longitudinal flagellum is at the posterior third of the cell, at the upper end of the open portion of the sulcus. This is in contrast to *A. klebsii* Kofoid & Swezy, a species in which the longitudinal flagellum originates near the anterior end of the hypocone (Taylor 1971). The absence of division cysts separates it from *A. steinii* (Stein 1883; Murray *et al.* 2004). Cell surface morphology, specifically the absence of scales, separate it from *A. paucianulatum, A. theodorei, A. massartii* and *A.* cf. *massartii* (Murray *et al.* 2004; Lee *et al.* 2013; Karafas *et al.* 2017). In addition, its large cell size does not overlap with that of most other species: *A. carterae, A. massartii, A.* cf. *massartii, A. thermaeum, A.* cf. *thermaeum, A. pseudomassartii, A. theodorei, A. fijiense* and *A. trulla* (Flø Jørgensen *et al.* 2004; Murray *et al.* 2004; Dolapsakis & Economou-Amilli 2009; Lee *et al.* 2013; Karafas *et al.* 2017). The autotrophic nature of *A. uduigamense* distinguishes it from *A. incoloratum*, which does not contain chloroplasts (Campbell 1973). Loss and reacquisition of phototrophy in dinoflagellates is not rare (Dorrell & Howe 2015). However, taking into consideration previous studies (Flø Jørgensen *et al.* 2004; Karafas *et al.* 2017), the long branches in the 28S tree in this study may have contributed to the grouping of *A. uduigamense, Amphidinium* sp. strain AmGMM3 and *A. incoloratum*. In addition, the lack of

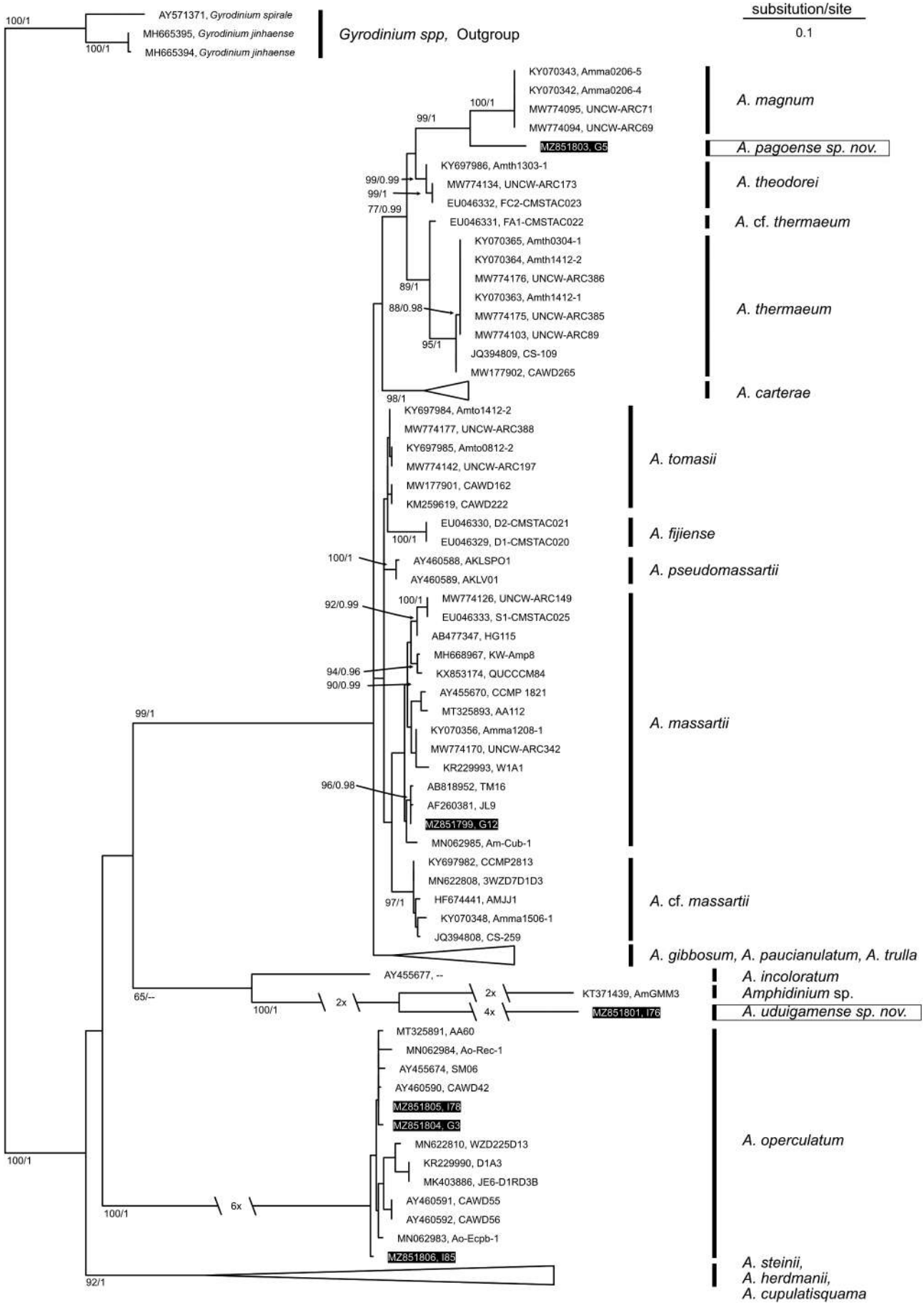

Fig. 41. Maximum likelihood phylogenetic tree inferred from the 28S rRNA gene. Bootstrap support lower than 60 and Bayesian posterior probability values lower than 95% are not displayed. Sequences originated from this study are written in white within black rectangles. Fast evolving taxa have truncated branches, reduced lengths indicated in branch. White triangles are collapsed taxa.

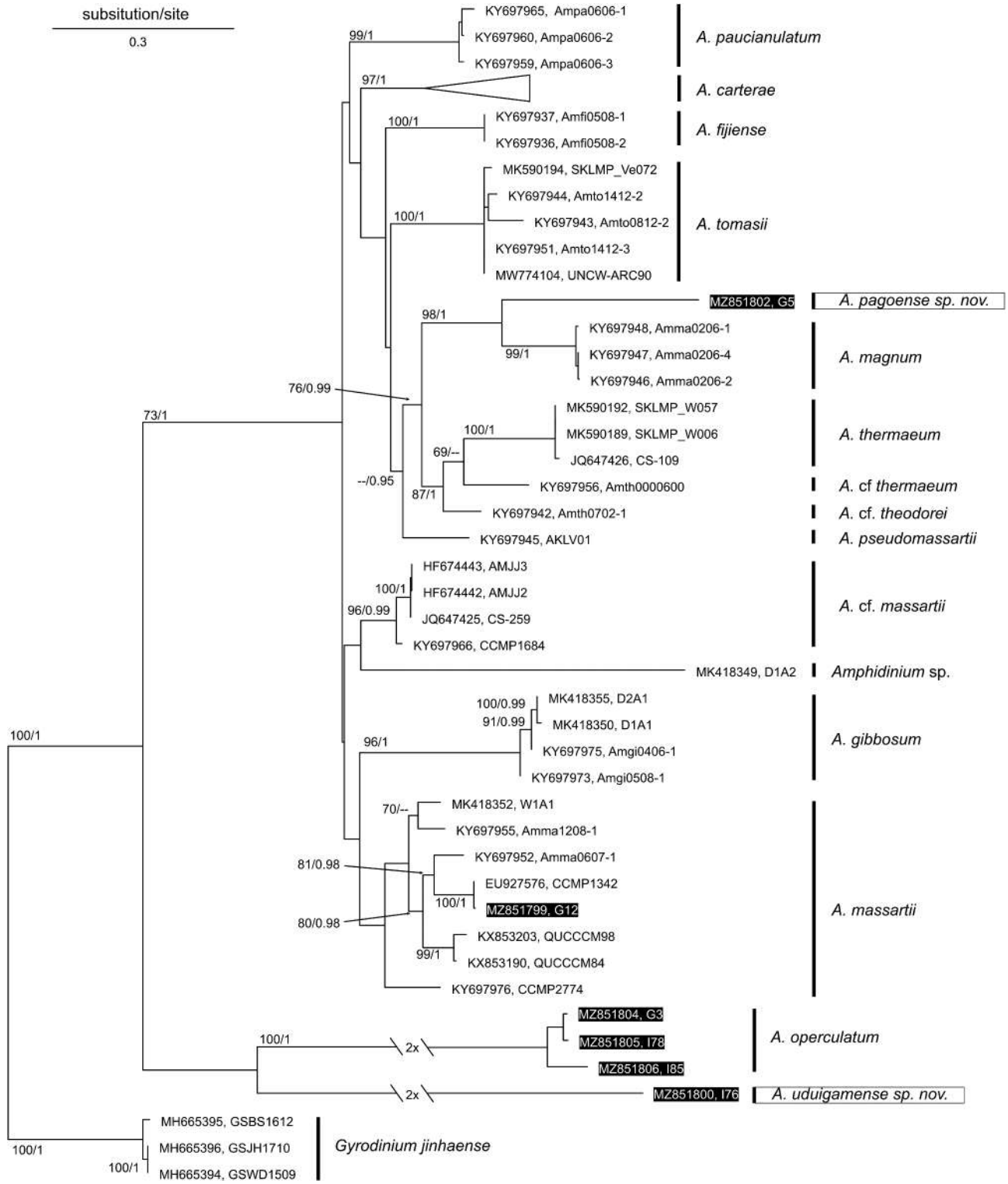

Fig. 42. Maximum likelihood phylogenetic tree inferred from the ITS rRNA gene region. Bootstrap support lower than 60 and Bayesian posterior probability values lower than 95% are not displayed. Sequences originated from this study are written in white within black rectangles. Fast evolving taxa have truncated branches, reduced lengths indicated in branch. White triangles are collapsed taxa.

ITS sequences for *Amphidinium* sp. strain AmGMM3 and *A. incoloratum* does not allow us to draw a definitive conclusion about their phylogenetic relationships. More informative gene sequences would be required to properly elucidate their phylogenetic relationship.

Both *A. uduigamense* and *A. pagoense* can be distinguished using morphological characters. However, species like *A. carterae, A. massartii* and *A. operculatum* have high genetic diversity, yet seem to be morphologically stagnant (Flø Jørgensen *et al.* 2004; Murray *et al.* 2004; Baig *et al.* 2006; Lee *et al.* 2013). Analysis of

Table 2. Pairwise distance of 28S rRNA gene of *Amphidinium*. Bold numbers indicate intraspecific distances. Divergence is reported as substitutions per site.

	1	2	3	4	5	6	7	8	9
1 *A. pagoense sp. nov.*	**na**								
2 *A. magnum*	0.080	**0.001**							
3 *A. theodorei*	0.093	0.085	**0.006**						
4 *A.* cf. *thermaeum*	0.100	0.104	0.059	**na**					
5 *A. uduigamense sp. nov.*	0.327	0.335	0.307	0.316	**na**				
6 *Amphidinium* sp. strain AmGMM3	0.310	0.321	0.302	0.305	0.292	**na**			
7 *A. incoloratum*	0.244	0.253	0.241	0.230	0.316	0.302	**na**		
8 *A. carterae*	0.131	0.127	0.081	0.090	0.329	0.312	0.235	**0.019**	
9 *A.* cf. *massartii*	0.124	0.119	0.083	0.084	0.343	0.339	0.253	0.080	**0.005**
10 *A. fijiense*	0.113	0.109	0.065	0.079	0.318	0.310	0.241	0.069	0.052
11 *A. gibbosum*	0.145	0.143	0.110	0.115	0.333	0.310	0.242	0.117	0.114
12 *A. herdmanii*	0.255	0.260	0.248	0.248	0.366	0.365	0.270	0.254	0.267
13 *A. massartii*	0.116	0.112	0.079	0.078	0.329	0.313	0.235	0.071	0.042
14 *A. operculatum*	0.338	0.352	0.339	0.337	0.414	0.425	0.383	0.343	0.342
15 *A. paucianulatum*	0.145	0.134	0.094	0.096	0.348	0.323	0.240	0.087	0.076
16 *A. pseudomassartii*	0.109	0.105	0.054	0.066	0.325	0.319	0.239	0.066	0.048
17 *A. steinii*	0.211	0.222	0.203	0.212	0.348	0.337	0.242	0.211	0.221
18 *A. thermaeum*	0.126	0.128	0.080	0.042	0.332	0.323	0.245	0.114	0.105
19 *A. tomasii*	0.121	0.115	0.063	0.076	0.367	0.348	0.265	0.096	0.061
20 *A. trulla*	0.135	0.130	0.106	0.114	0.324	0.321	0.243	0.106	0.106
21 *A. cupulatisquama*	0.264	0.266	0.255	0.255	0.388	0.359	0.283	0.267	0.273

	10	11	12	13	14	15	16	17	18	19	20	21
1 *A. pagoense sp. nov.*												
2 *A. magnum*												
3 *A. theodorei*												
4 *A.* cf. *thermaeum*												
5 *A. uduigamense sp. nov.*												
6 *Amphidinium* sp. strain AmGMM3												
7 *A. incoloratum*												
8 *A. carterae*												
9 *A.* cf. *massartii*												
10 *A. fijiense*	**0.003**											
11 *A. gibbosum*	0.100	**0.007**										
12 *A. herdmanii*	0.241	0.260	**0.013**									
13 *A. massartii*	0.050	0.107	0.256	**0.019**								
14 *A. operculatum*	0.341	0.347	0.369	0.339	**0.038**							
15 *A. paucianulatum*	0.080	0.108	0.270	0.074	0.356	**0.000**						
16 *A. pseudomassartii*	0.046	0.102	0.244	0.044	0.343	0.071	**0.000**					
17 *A. steinii*	0.203	0.218	0.209	0.208	0.373	0.220	0.203	**0.026**				
18 *A. thermaeum*	0.098	0.135	0.273	0.104	0.347	0.118	0.090	0.228	**0.002**			
19 *A. tomasii*	0.061	0.123	0.287	0.058	0.361	0.091	0.040	0.245	0.099	**0.007**		
20 *A. trulla*	0.099	0.118	0.259	0.092	0.354	0.105	0.100	0.223	0.140	0.112	**0.019**	
21 *A. cupulatisquama*	0.256	0.257	0.191	0.262	0.371	0.271	0.258	0.222	0.274	0.298	0.260	**na**

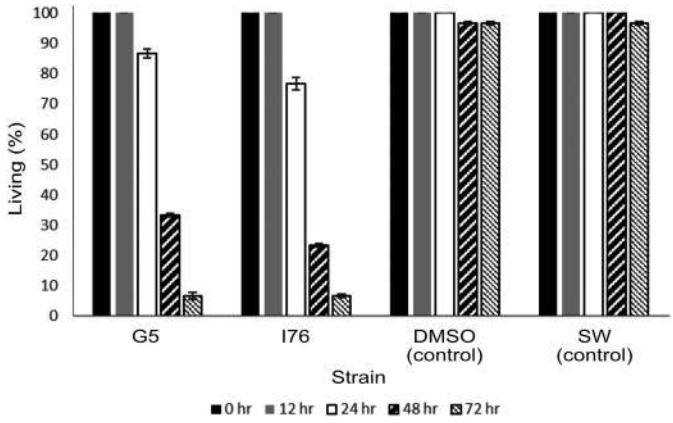

Fig. 43. Percentage of living *Artemia* larvae after a period of 12, 48 and 72 h, following the addition of *Amphidinium pagoense sp. nov.* (G5) and *A. uduigamense* sp. nov. (I76) extracts. Negative control: DMSO and seawater (SW).

ITS2 secondary structure has been used to show that isolates of *A. carterae* and *A. massartii* fall into distinct clades (Lee *et al.* 2013; Karafas *et al.* 2017). Many isolates within the *A. massartii* species complex are morphologically similar; however, it appears possible that independent convergence to this general form has occurred multiple times (Murray *et al.* 2004; Lee *et al.* 2013; Karafas *et al.* 2017). The *A. massartii* species complex is an example that highlights the importance of using molecular data when identifying species of *Amphidinium* that are challenging to delimitate based solely on appearance. In the results from our molecular phylogenetic analyses, there was a main clade of *A. massartii* composed of isolates from the Persian Gulf, Japan, Mexico, Palmyra Atoll, China, Florida and Belize (Flø Jørgensen *et al.* 2004; Al-Muftah *et al.* 2016; Karafas *et al.* 2017); another clade (*A.* cf. *massartii*) was also recovered, and was comprised of isolates from Australia, Korea and Fiji (Lee *et al.* 2013; Karafas *et al.* 2017). These phylogenetic results suggest that the current concept of *A. massartii* is likely to include more than one species, and that these species have broad and overlapping geographic distributions. Isolating and establishing culture strains (similar to the one established from Guam in this study) will better our understanding of the global distribution of this group, and shed light on the probable cryptic speciation among its lineages.

Past work on isolates of *A. operculatum* originating from different sampling locations have shown that this species has similar morphology, despite high intraspecific genetic variation (Grell & Wohlfarth-Bottermann 1957; Murray *et al.* 2004, 2012). Similarly, our phylogenetic analyses showed that the Okinawa isolate from this study (strain I85) is consistently excluded from other isolates of *A. operculatum*, including strains G3 and I78. Interestingly, strains I78 and I85 were both isolated from relatively close sampling sites on Okinawa, and G3 was isolated more than 2000 km away on Guam. Though it has low support, it could indicate cryptic speciation. Taking into consideration the high genetic diversity and widespread distribution of *A. operculatum*, the addition of more ITS sequences from different strains of *A. operculatum* will allow for the implementation of additional analytical techniques like compensatory base changes of ITS2 rRNA secondary structures to characterize this clade (Karafas *et al.* 2017).

In this study, the two new species, *A. pagoense* and *A. uduigamense,* displayed toxicity in an *Artemia* bioassay—similar to most other species of *Amphidinium* (Murray *et al.* 2015; Karafas *et al.* 2017; Mejía-Camacho *et al.* 2021). Production of natural compounds by *Amphidinium* has been of interest for the usage of their bioactive properties against marine invertebrates, fungi, bacteria and tumour cell lines (Bauer *et al.* 1995; Kobayashi 2008; Espiritu *et al.* 2017; Martínez *et al.* 2019). Variations in toxic effects between different assays have been observed (Pagliara & Caroppo 2012). For example, *Amphidinium* cell lysate showed toxicity against marine invertebrates and human red blood cells (Pagliara & Caroppo 2012). However, it has also been shown that amphidinol 22 is effective against cancer cell lines and fungi, but not against bacteria (Martínez *et al.* 2019). The effect of cell lysates can also differ between cancer cell lines (Mejía-Camacho *et al.* 2021). Both *A. pagoense* and *A. uduigamense* have shown toxicity against *Artemia*, but without performing different assays this alone may not be sufficient to draw conclusions on its chemical effects.

ACKNOWLEDGEMENTS

We would like to thank the OIST Imaging Section for providing access to SEM equipment and Mr. Sasaki for support, as well as the Hokkaido University School of Agriculture for providing access to their EM Facilities.

DISCLOSURE STATEMENT

No potential conflict of interest was reported by the authors.

FUNDING

Financial support for this project was provided by Japanese Society for the Promotion of Science (JSPS) [Grants 18K14774 and PG6R180004 to KCW]. The Institute for the Advancement of Higher Education at Hokkaido University provided additional funding and admissive support to KCW. Sampling for this project was supported by the University of Guam Marine Laboratory.

REFERENCES

Al-Muftah A., Selwood A.I., Foss A.J., Al-Jabri H.M.S.J., Potts M. & Yilmaz M. 2016. Algal toxins and producers in the marine waters of Qatar, Arabian Gulf. *Toxicon* 122: 54–66. DOI: 10.1016/j.toxicon.2016.09.016.

Baig H.S., Saifullah S.M. & Dar A. 2006. Occurrence and toxicity of *Amphidinium carterae* Hulburt in the North Arabian Sea. *Harmful Algae* 5: 133–140. DOI: 10.1016/j.hal.2005.06.010.

Bates H.A., Kostriken R. & Rapoport H. 1978. The occurrence of saxitoxin and other toxins in various dinoflagellates. *Toxicon* 16: 595–601. DOI: 10.1016/0041-0101(78)90187-3.

Bauer I., Maranda L., Young K.A., Shimizu Y., Fairchild C., Cornell L., Macbeth J. & Huang S. 1995. Isolation and structure of caribenolide I, a highly potent antitumor macrolide from a cultured free-swimming Caribbean dinoflagellate, *Amphidinium* sp. S1-36-5. *Journal of Organic Chemistry* 60: 1084–1086. DOI: 10.1021/jo00109a050.

Biecheler B. 1952. Recherches sur les Péridiniens. *Bulletin Biologique de la France et de la Belgique, Supplément* 36: 1–149.

Campbell P.H. 1973. *Studies on brackish water phytoplankton*. Sea Grant Publication UNC-SG-73-07, University of North Carolina, Chapel Hill, North Carolina, USA. 403 pp.

Castresana J. 2000. Selection of conserved blocks from multiple alignments for their use in phylogenetic analysis. *Molecular Biology and Evolution* 17: 540–552. DOI: 10.1093/oxfordjournals.molbev.a026334.

Claparède E. & Lachmann J. 1859. Études sur les Infusoires et les Rhizopodes. *Mémoires de l'Institut National Genevois* 6: 261–482, pls 14–24.

Daugbjerg N., Hansen G., Larsen J. & Moestrup Ø. 2000. Phylogeny of some of the major genera of dinoflagellates based on ultrastructure and partial LSU rDNA sequence data, including the erection of three new genera of unarmoured dinoflagellates. *Phycologia* 39: 302–317. DOI: 10.2216/i0031-8884-39-4-302.1.

Dodge J.D. 1982. *Marine dinoflagellates of the British Isles*. Her Majesty's Stationery Office, London, UK. 303 pp.

Dolapsakis N.P. & Economou-Amilli A. 2009. A new marine species of *Amphidinium* (Dinophyceae) from Thermaikos Gulf, Greece. *Acta Protozoologica* 48: 153–170.

Dorrell R.G. & Howe C.J. 2015. Integration of plastids with their hosts: lessons learned from dinoflagellates. *Proceedings of the National Academy of Sciences of the USA* 112: 10247–10254. DOI: 10.1073/pnas.1421380112.

Edgar R.C. 2004. MUSCLE: multiple sequence alignment with high accuracy and high throughput. *Nucleic Acids Research* 32: 1792–1797. DOI: 10.1093/nar/gkh340.

Espiritu R.A., Tan M.C.S. & Oyong G.G. 2017. Evaluation of the anti-cancer potential of amphidinol 2, a polyketide metabolite from the marine dinoflagellate *Amphidinium klebsii*. *Jordan Journal of Biological Sciences* 10: 297–302.

Flø Jørgensen M., Murray S. & Daugbjerg N. 2004. *Amphidinium* revisited. I. Redefinition of *Amphidinium* (Dinophyceae) based on cladistic and molecular phylogenetic analyses. *Journal of Phycology* 40: 351–365. DOI: 10.1111/j.1529-8817.2004.03131.x.

Grell K.G. & Wohlfarth-Bottermann K.E. 1957. Licht- und elektronenmikroskopische Untersuchungen an dem Dinoflagellaten *Amphidinium elegans* n. sp. *Zeitschrift für Zellforschung und Mikroskopische Anatomie* 47: 7–17. DOI:10.1007/BF00340000.

Karafas S., Teng S.T., Leaw C.P. & Alves-de-Souza C. 2017. An evaluation of the genus *Amphidinium* (Dinophyceae) combining evidence from morphology, phylogenetics, and toxin production, with the introduction of six novel species. *Harmful Algae* 68: 128–151. DOI: 10.1016/j.hal.2017.08.001.

Kobayashi J. 2008. Amphidinolides and its related macrolides from marine dinoflagellates. *Journal of Antibiotics* 61: 271–284. DOI: 10.1038/ja.2008.39.

Kobayashi J. & Tsuda M. 2004. Amphidinolides, bioactive macrolides from symbiotic marine dinoflagellates. *Natural Product Reports* 21: 77–93. DOI: 10.1039/B310427N.

Kumar S., Stecher G., Li M., Knyaz C. & Tamura K. 2018. MEGA X: molecular evolutionary genetics analysis across computing platforms. *Molecular Biology and Evolution* 35: 1547–1549. DOI: 10.1093/molbev/msy096.

Leander B.S., Harper J.T. & Keeling P.J. 2003. Molecular phylogeny and surface morphology of marine aseptate gregarines (Apicomplexa): *Selenidium* spp. and *Lecudina* spp. *Journal of Parasitology* 89: 1191–1205. DOI: 10.1645/GE-3155.

Lee K.H., Jeong H.J., Park K., Kang N.S., Du Y.Y., Lee M.J., Lee J.W., Lee S., Kim T., Kim H.S. *et al.* 2013. Morphology and molecular characterization of the epiphytic dinoflagellate *Amphidinium massartii*, isolated from the temperate waters off Jeju Island, Korea. *Algae* 28: 213–231. DOI: 10.4490/algae.2013.28.3.213.

Maddison W.P. & Maddison D.R. 2021. Mesquite: amodular system for evolutionary analysis, version 3.70. http://www.mesquiteproject.org.

Martínez K.A., Lauritano C., Druka D., Romano G., Grohmann T., Jaspars M., Martín J., Díaz C., Cautain B., de la Cruz M. *et al.* 2019. Amphidinol 22, a new cytotoxic and antifungal amphidinol from the dinoflagellate *Amphidinium carterae*. *Marine Drugs* 17: Article 385. DOI: 10.3390/md17070385.

Mejía-Camacho A.L., Durán-Riveroll L.M. & Cembella A.D. 2021. Toxicity bioassay and cytotoxic effects of the benthic marine dinoflagellate *Amphidinium operculatum*. *Journal of Xenobiotics* 11: 33–45. DOI: 10.3390/jox11020003.

Moestrup Ø. & Calado A.J. 2018. Dinophyceae. In: *Freshwater Flora of Central Europe – Süßwasserflora von Mitteleuropa*, vol. 6, ed. 2 (Ed. by B. Büdel, G. Gärtner, L. Krienitz & M. Schagerl). Springer-Verlag, Berlin, Germany. 561 pp.

Morsy N., Konoki K., Houdai T., Matsumori N., Oishi T., Murata M. & Aimoto S. 2008. Roles of integral protein in membrane permeabilization by amphidinols. *Biochimica et Biophysica Acta* 1778: 1453–1459. DOI: 10.1016/j.bbamem.2008.01.018.

Murray S. & Patterson D.J. 2002. The benthic dinoflagellate genus *Amphidinium* in south-eastern Australian waters, including three new species. *European Journal of Phycology* 37: 279–298. DOI: 10.1017/S0967026202003591.

Murray S., Flø Jørgensen M., Daugbjerg N. & Rhodes L. 2004. *Amphidinium* revisited. II. Resolving species boundaries in the *Amphidinium operculatum* species complex (Dinophyceae), including the descriptions of *Amphidinium trulla* sp. nov. and *Amphidinium gibbosum* comb. nov. *Journal of Phycology* 40: 366–382. DOI: 10.1046/j.1529-8817.2004.03132.x.

Murray S.A., Garby T., Hoppenrath M. & Neilan B.A. 2012. Genetic diversity, morphological uniformity and polyketide production in dinoflagellates (*Amphidinium*, dinoflagellata). *PLOS One* 7: Article e38253. DOI: 10.1371/journal.pone.0038253.

Murray S.A., Kohli G.S., Farrell H., Spiers Z.B., Place A.R., Dorantes-Aranda J.J. & Ruszczyk J. 2015. A fish kill associated with a bloom of *Amphidinium carterae* in a coastal lagoon in Sydney, Australia. *Harmful Algae* 49: 19–28. DOI: 10.1016/j.hal.2015.08.003.

Nakajima I., Oshima Y. & Yasumoto T. 1981. Toxicity of benthic dinoflagellates in Okinawa. *Bulletin of the Japanese Society of Scientific Fisheries (Nippon Suisan Gakkaishi)* 47: 1029–1033. DOI: 10.2331/suisan.47.1029.

Nguyen L.-T., Schmidt H.A., Von Haeseler A. & Minh B.Q. 2014. IQ-TREE: a fast and effective stochastic algorithm for estimating maximum-likelihood phylogenies. *Molecular Biology and Evolution* 32: 268–274. DOI: 10.1093/molbev/msu300.

Pagliara P. & Caroppo C. 2012. Toxicity assessment of *Amphidinium carterae, Coolia* cfr. *monotis* and *Ostreopsis* cfr. ovata (Dinophyta) isolated from the northern Ionian Sea (Mediterranean Sea). *Toxicon* 60: 1203–1214. DOI: 10.1016/j.toxicon.2012.08.005.

Rambaut A., Drummond A.J., Xie D., Baele G. & Suchard M.A. 2018. Posterior summarization in Bayesian phylogenetics using Tracer 1.7. *Systematic Biology* 67: 901–904. DOI: 10.1093/sysbio/syy032.

Rhodes L.L., Smith K., Papiol G.G., Adamson J., Harwood T. & Munday R. 2014. Epiphytic dinoflagellates in sub-tropical New Zealand, in particular the genus *Coolia* Meunier. *Harmful Algae* 34: 36–41. DOI: 10.1016/j.hal.2014.02.004.

Ronquist F. & Huelsenbeck J.P. 2003. MrBayes 3: Bayesian phylogenetic inference under mixed models. *Bioinformatics* 19: 1572–1574. DOI: 10.1093/bioinformatics/btg180.

Satake M., Murata M., Yasumoto T., Fujita T. & Naoki H. 1991. Amphidinol, a polyhydroxypolyene antifungal agent with an unprecedented structure, from a marine dinoflagellate, *Amphidinium klebsii*. *Journal of the American Chemical Society* 113: 9859–9861. DOI: 10.1021/ja00026a027.

Steidinger K.A. & Tangen K. 1997. Dinoflagellates. In: *Identifying marine phytoplankton* (Ed. by C.R. Tomas), pp 387–584. Academic Press, St Petersburg, Florida, USA.

Stein F. 1883. *Der Organismus der Infusionsthiere. . . III. Die Naturgeschichte der Flagellaten oder Geisselinfusorien. II Hälfte. Naturgeschichte der arthrodelen Flagellaten. Einleitung und Erklärung der Abbildungen*. Wilhelm Engelmann, Leipzig, Germany. 30 pp, 25 pls.

Talavera G. & Castresana J. 2007. Improvement of phylogenies after removing divergent and ambiguously aligned blocks from protein sequence alignments. *Systematic Biology* 56: 564–577. DOI: 10.1080/10635150701472164.

Taylor D.L. 1971. Taxonomy of some common *Amphidinium* species. *British Phycological Journal* 6: 129–133. DOI: 10.1080/00071617100650151.

Yasumoto T., Seino N., Murakami Y. & Murata M. 1987. Toxins produced by benthic dinoflagellates. *Biological Bulletin* 172: 128–131. DOI: 10.2307/1541612.